Tubulin Oligomers and Microtubule Assembly Studied by Time-Resolved X-ray Scattering: Separation of Prenucleation and Nucleation Events†

U. Spann,‡ W. Renner,‡,§ E.-M. Mandelkow,‖ J. Bordas,⊥ and E. Mandelkow*,‖

Department of Biophysics, Max-Planck-Institut for Medical Research, D-6900 Heidelberg, FRG, Max-Planck-Unit for Structural Molecular Biology, D-2000 Hamburg 52, FRG, and MRC-SERC Biology Support Laboratory, Daresbury Laboratory, Warrington WA4 4AD, U.K.

Received June 5, 1986; Revised Manuscript Received September 24, 1986

ABSTRACT: This paper describes a time-resolved X-ray scattering study of microtubule assembly by synchrotron radiation. The method is complementary to light scattering but allows a better distinction between oligomeric and polymeric assembly states. With an improved rapid temperature jump device, it is shown that temperature-induced microtubule assembly is preceded by prenucleation and nucleation events involving oligomers of tubulin, in analogy with earlier results from near-equilibrium temperature scans. In general, the two phases closely overlap, but in certain conditions they can be observed separately. The prenucleation events seen by X-rays can be described as a rapid temperature-dependent equilibrium, with ring oligomers dissociating into smaller oligomers and subunits at elevated temperature. Different solution conditions affect mainly the time lag between the prenucleation and nucleation phases; this in turn determines the apparent magnitude of the prenucleation steps. By contrast, the temperature dependence of the equilibrium between the prenucleation oligomers shows little influence on solution conditions. The results suggest that the ring-forming and tubule-forming assembly modes of tubulin are governed by different interactions between subunits, although they may be based on a pool of similar intermediates.

In earlier reports we have described the process of temperature-induced microtubule assembly as seen by time-resolved X-ray scattering (Mandelkow et al., 1980, 1983; Bordas et al., 1983). The observed states could be broadly subdivided into the initial (cold) state, prenucleation events, nucleation, elongation, final (warm) state, and postassembly events. The initial cold state was characterized by a mixture of rings, oligomers, and dimers. Prenucleation events were seen as an undershoot in scattering that reflected the breakdown of rings and oligomers into smaller units. Nucleation was interpreted in terms of an association of oligomers, while the final warm state was dominated by the scattering from microtubules. Oligomers were observed not only with MAP[1]-containing microtubule protein but also with purified tubulin that lacked the rings typical of cold microtubule protein. Both the ring and nonring oligomers appeared to consist of short stretches of protofilaments, and the structural and kinetic evidence suggested that oligomeric states of tubulin were important for microtubule assembly.

Under the experimental conditions employed previously, there was an overlap of the prenucleation and nucleation events following a temperature jump from 4 to 37 °C, such that the magnitudes and rates of the individual phases could not be analyzed separately. In this paper, we describe experiments designed to separate the prenucleation events from the subsequent microtubule assembly. This can be achieved, for example, by lowering the pH and the ionic strength. Within the time resolution of the temperature jump (a few seconds), the oligomeric forms appear to be in a rapid temperature-dependent equilibrium, independent of whether microtubule assembly is rapid or slow. The results suggest that the transitions between prenucleation oligomers occur independently of the interactions between the nucleating oligomers.

Materials and Methods

Protein Preparation. Microtubule protein was prepared by one of the temperature cycle methods [e.g., Borisy et al. (1975)], with modifications. The reassembly buffer was usually 0.1 M PIPES, pH between 6.9 and 6.5, containing 1 mM each of $MgSO_4$, DTT, EGTA, and GTP. For certain experiments the ionic strength was varied by reducing the buffers and/or adding salts. At pH 6.9 the ionic strength is roughly 1.6 times the concentration of PIPES buffer (at room temperature), at pH 6.6 the factor is about 1.4, and at pH 7.5 the factor is about 1.9. Protein concentrations ranged up to 30 mg/mL. The protein was prepared in standard conditions (0.1 M buffer strength), aliquoted, and frozen in liquid nitrogen. Prior to the experiment, the samples were unfrozen and used as such or carried through another cycle (e.g., in order to change assembly buffers). The protein preparations were usually checked by gel electrophoresis and electron microscopy (thin sectioning or negative staining). Protein concentrations were determined by a modified Lowry procedure (Schachterle & Pollack, 1973), with bovine serum albumin as a standard.

Time-Resolved X-ray Scattering using Synchrotron Radiation. The X-ray experiments were performed at the EMBL Outstation at DESY, Hamburg, as described (Mandelkow et al., 1980; Bordas et al., 1983), with instrument X31 or X11 (Koch & Bordas, 1983; Hendrix et al., 1979), position-sensitive

† This work was supported by the Max-Planck-Gesellschaft (MPG), the European Molecular Biology Laboratory (EMBL), the Deutsche Forschungsgemeinschaft (DFG), the Commission of the European Communities (CODEST), and the Bundesministerium für Forschung und Technologie (BMFT).

* Author to whom correspondence should be addressed.

‡ Max-Planck-Institut for Medical Research.

§ Present address: Institut für Software-Technik, 6100 Darmstadt, FRG.

‖ Max-Planck-Unit for Structural Molecular Biology.

⊥ MRC-SERC Biology Support Laboratory.

[1] Abbreviations: DTT, dithiothreitol; EGTA, ethylene glycol bis(2-aminoethyl ether)-*N*,*N*,*N*′,*N*′-tetraacetic acid; GTP, guanosine 5′-triphosphate; MAPs, microtubule-associated proteins; PIPES, piperazine-*N*,*N*′-bis(2-ethanesulfonic acid).

0006-2960/87/0426-1123$01.50/0

detectors [linear detector, see Gabriel (1977); or a quadrant detector integrating the circularly symmetric solution pattern over an angle of 90°, J. Hendricks and J. Bordas, unpublished data], and a fast data acquisition system (Bordas et al., 1980). Assembly and disassembly were induced by temperature jumps between 0–5 and 35–37 °C (half-time 4–10 s, depending on the settings of the thermostats) with the T-jump device described elsewhere (Renner et al., 1983). Reciprocal spacings were calibrated with respect to the collagen reflections from a sample of cornea or tendon. The scattering curves were normalized with respect to the incident intensity measured by an ionization chamber just upstream from the specimen chamber.

Data Analysis and Model Calculations. The final data reduction and analysis was done off-line on a Norsk Data 100/500 computer, following the procedures of Koch and Bendall (1981). The observed intensities were corrected for background (measured from a buffer-filled cell), detector response, and variations in incident intensity due to the decay of the current in the storage ring. The scattering data were interpreted as described (Mandelkow et al., 1983; Bordas et al., 1983).

Figure 1 shows calculated scattering curves of several representative model structures, including microtubules, rings, protofilament fragments, and tubulin dimers. The curves are normalized to the same total protein concentration so that the forward scattering ($S = 0$) represents the degree of polymerization. Microtubules show the highest central scatter and several subsidiary maxima separated by clear minima. Rings have a lower central scatter and side maxima that are approximately out of phase with respect to those of microtubules. In both cases, the positions of the first side maxima are close to $S = 1.22/D$, where D is the mean diameter of the respective hollow cylinders. Since microtubules have smaller diameters than rings, their subsidiary peaks occur at higher S values. By contrast, both tubulin dimers and short protofilament fragments show smoothly decaying scattering curves. In practice, one usually observes a mixture of several types of aggregate, especially at low temperature where rings, oligomers, and dimers are in equilibrium. The minimum preceding the first maximum of microtubules is particularly sensitive to the presence of oligomeric structures.

Because of the beam stop and parasitic scatter, the lowest observable S values are around 0.01 nm^{-1}. In the following, the intensity integrated between about 0.01 and 0.015 nm^{-1} will be referred to as "central scatter" for brevity (note that this is only an approximation to the forward scattering), integration between about 0.025 and 0.035 nm^{-1} yields the "ring scatter" since this overlaps with the first side maximum of the form factor of rings, and the region around 0.045–0.05 nm^{-1} will be called "microtubule scatter" (see arrows C, R, and M in Figure 1). The time-dependent changes in these regions allow one to assess the main features of assembly and disassembly (e.g., Figures 2a,c). For example, a rise in the central scatter indicates overall assembly, a rise in the microtubule scatter usually means formation of microtubules, and a rise in the ring scatter may mean ring formation and/or other structures (e.g., oligomers). The actual structures present may be analyzed from the scattering curves or difference plots at given time points (e.g., Figures 2b and 3b).

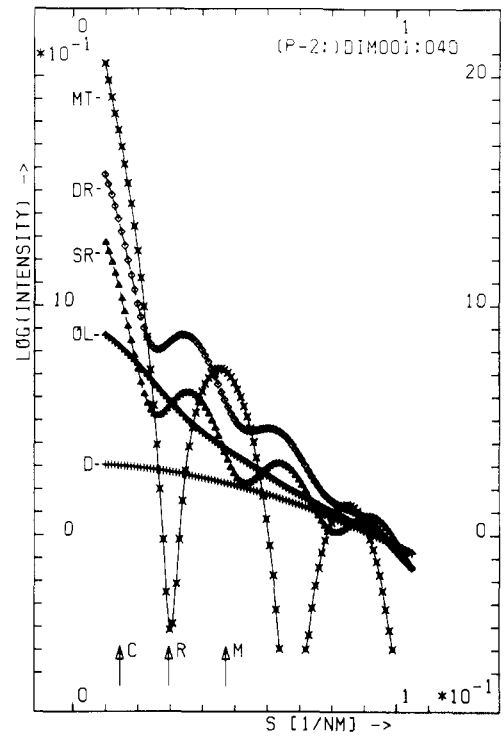

FIGURE 1: Theoretical scattering curves of model structures. The curves were calculated on the basis of Debye's formula, with spheres of 4-nm diameter to represent the protein subunits. The scattering of mixtures of aggregates can be calculated from $I(S,t) = \sum_k x_k(t) p_k i_k(S)$, where the index k refers to the species of aggregate, $x_k(t)$ is the fraction of subunits assembled into the species k, p_k is the degree of polymerization, $i_k(S)$ is the form factor shown in the figure, and $S = 2 \sin \theta/\lambda$ is the Bragg scattering vector [for details, see Mandelkow et al. (1983)]. (Top to bottom on left-hand side) Microtubule with 13 protofilaments of mean diameter 26 nm (MT); double concentric ring of 36-nm mean diameter (40 nm for outer, 32 nm for inner turn, DR), with subunits spaced 4 nm apart (=coiled protofilaments); single ring of 36-nm mean diameter (SR), oligomer consisting of four dimers (=protofilament fragment, OL), and dimer (D). Note that the central scatter (left) increases with the degree of polymerization; the side maxima of rings and microtubules are roughly in antiphase; oligomers and dimers have smoothly decaying scattering curves, with the former contributing noticeably at small angles. The model diameters are close to but not identical with the observed ones. The arrows marked C, R, and M indicate the regions sensitive to overall assembly (central scatter, C), rings (R), or microtubules (M). They are used to monitor the time dependence of the reactions.

RESULTS

Prenucleation and Assembly Phases in Standard Buffer Conditions. Figure 2 illustrates one cycle of assembly and disassembly of microtubule protein in standard buffer conditions (0.1 M PIPES reassembly buffer, pH 6.9). The projection plot (Figure 2a) shows the time dependence of the scattering traces. Representative curves from the initial (cold) and the polymerized state (warm) are shown in Figure 2b. The initial state has a low central scatter (left) and the side maxima typical of rings of diameter 36 nm; the polymerized state has a higher central scatter and the side maxima characteristic of microtubules (weight-average mean diameter 25 nm). A detailed comparison with the calculated scattering of model structures shows that most observed traces can only be explained if one allows for contributions from other structures [e.g., oligomers, dimers, MAPs; see Bordas et al. (1983)]. At high temperatures, the patterns are dominated by the scattering from microtubules, with a minor contribution from species that are best explained in terms of oligomers and/or MAPs that contribute mainly at very small scattering angles and fill in the minima of the microtubule trace. The scattering at low temperature can be modeled by mixtures of single and double concentric rings plus oligomers. The scattering from double rings has a higher first subsidiary peak but decays more quickly than the scattering from single rings (see Figure 1). As before, oligomeric species contribute mainly at small angles,

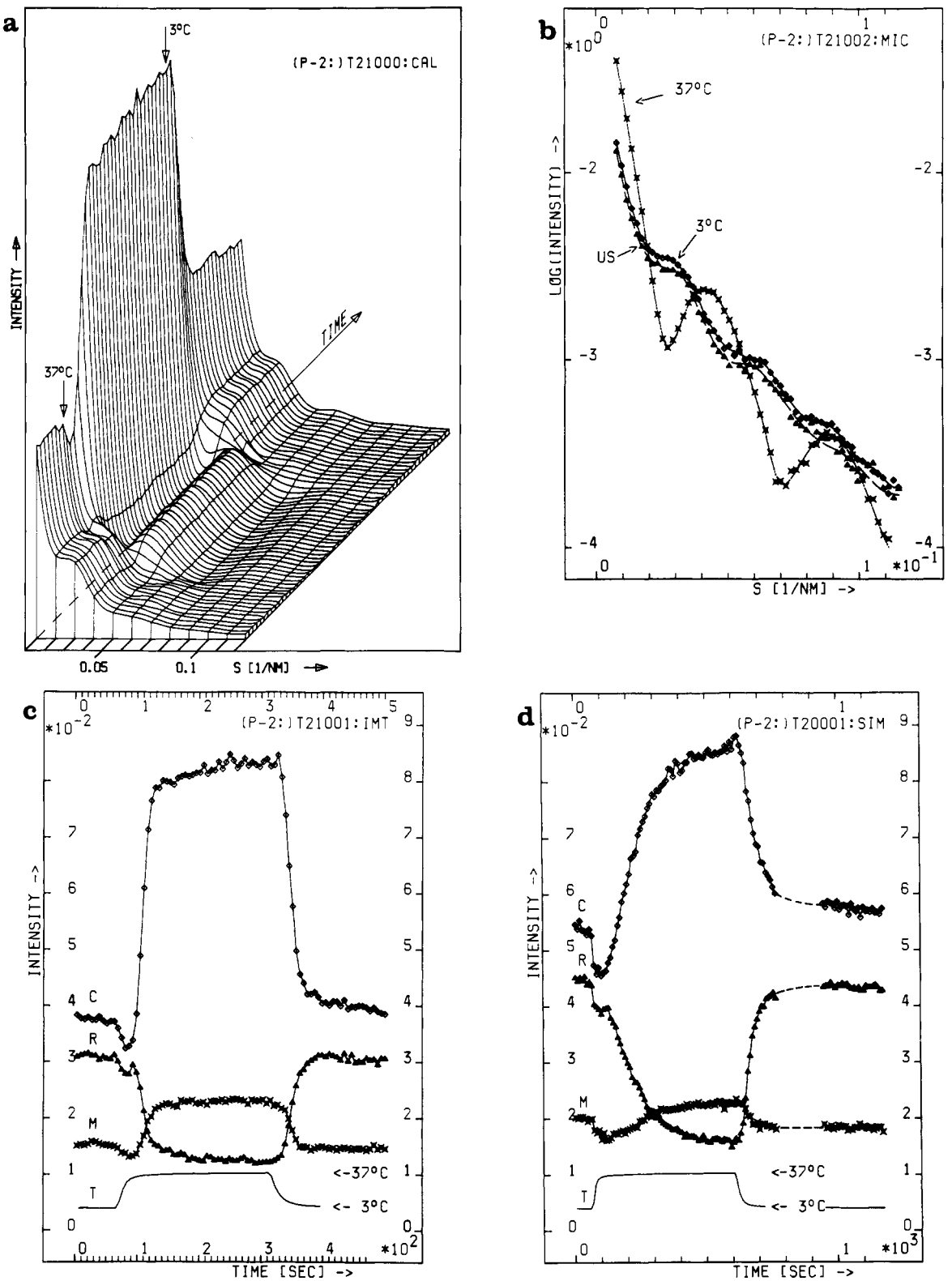

FIGURE 2: Microtubule assembly in 0.1 M PIPES buffer, pH 6.94. (a) Projection plot of control experiment T21.829. Microtubule protein C_3S-56, 30 mg/mL, with 1 mM EGTA, DTT, and $MgSO_4$ and 2 mM GTP. EMBL instrument X33, camera length 3 m, linear position-sensitive detector with 256 channels, 256 time frames of 3 s per run (only every third shown), temperature jumps from 3 (initial cold) to 37 °C, and return (arrows). Note the increase in central scatter during assembly and the change in side maxima. The scattering curves in this figure and elsewhere have been smoothed by cubic spline functions. (b) Selected scattering traces of experiment shown in (a) (T21.829, log of intensity vs. reciprocal spacing S). Diamonds = initial cold state (average of time frames 5–15, 3 °C) showing side maxima typical of rings (36-nm mean diameter); triangles = undershoot before onset of assembly (average of time frames 27–29, US) showing a decrease in the fraction of rings; crosses = warm state (average of time frames 94–104, 37 °C) showing side maxima typical of microtubules (25-nm weight-average mean diameter). Every second data point is shown. (c) Time course of scattered intensities in experiment T21.829. (Top to bottom) Central scatter (integrated from $S = 0.011$ to $S = 0.015$ nm^{-1}, C), ring scatter (0.023–0.031 nm^{-1}, R), microtubule scatter (0.041–0.051 nm^{-1}, M), and temperature (initial and final values 3 and 37 °C, T). Every second data point is shown. (d) Time course of intensities in experiment T19.829, plotted similarly to (c). Same protein preparation as in experiment T21.829 but stored on ice for 12 h. Note pronounced undershoot and reduced rates of assembly and disassembly [compared with (c)]. The dashed lines indicate an interruption of the experiment caused by saving data on disk and starting a new run. Every third data point is shown.

with radii of gyration on the order of 10 nm [determined from the slope of Guinier plots; see Guinier and Fournet (1955)]. The contribution from tubulin dimers is generally small and thus negligible within noise until one reaches higher scattering angles (second side maximum and beyond, see Figure 1). However, the presence of species with unknown form factors allows only an approximate quantitation of the individual components, especially at low temperature and during the assembly phase.

Figure 2c shows the time courses of the intensities in the regions designated in Figure 1 as central scatter (C), ring scatter (R), and microtubule scatter (M); the temperature (T) is shown in the bottom trace. They show the following features: After the upward temperature jump, the central scatter drops briefly to 87% of its initial value and then rises rapidly to twice its initial value, followed by a second slow rise (total increase 2.2-fold), and after the reverse T jump, the intensity drops in a biphasic manner and equilibrates 5% above its initial value. The microtubule scatter shows a similar behavior but with different amplitudes since the rise in polymerization is due to the formation of microtubules. The time course of the ring scatter is roughly the mirror image of the microtubule scatter since rings disappear when microtubules are formed and since the microtubule scatter has a minimum where the ring scatter has a peak (Figure 2b).

In this paper, we are particularly concerned with the small deviations from the initial level before and after assembly. The undershoot after the T jump up can be accounted for by the partial dissolution of rings; this feature is seen in all three time courses shown. The increase in the level after one cycle is seen mainly in the central scatter and is explained by nonring oligomers that reassemble into rings slowly or not at all.

In our previous studies employing moderate temperature jumps or slow temperature scans, we have concluded that tubulin oligomers (formed as breakdown products of the prenucleation ring dissolution) played a role in microtubule assembly. However, a puzzling aspect of the intensity undershoot representing this phase was its variability; it depended on protein preparation, solution parameters, initial conditions of assembly, etc. The undershoot is usually absent in solutions containing glycerol (which stabilizes rings and oligomers, not shown) or with samples of MAP-free tubulin (which contains small oligomers but not rings in our standard assembly buffer, to be described elsewhere).

The shape of the undershoot in Figure 2c suggests that one is observing a superposition of two events with opposite effects on the scattering. Thus, the amplitudes and rates of both reactions remain uncertain. We have therefore searched for conditions that allow the undershoot to be measured clearly without interference from the onset of assembly. An approximation to this condition is illustrated in Figure 2d. The curves were obtained with the same protein as before, except that it was left on ice for 12 h after unfreezing, rather than using it immediately as in Figure 2a. During this period, the GTP is slowly hydrolyzed, as measured by the gradual decay of polymerizability (a similar effect can be produced by adding GDP, and it can be reversed by adding GTP, as in Figure 2c). We note several differences in assembly behavior: Both assembly and disassembly are reduced, the rise of the central scatter is smaller than before (1.8-fold of the initial value), and the undershoot becomes very pronounced (down to 85% of initial value). More importantly, the undershoot appears to approach an equilibrium before assembly begins.

Several lessons can be learned from this experiment: (1) The apparent duration and magnitude of the undershoot are indeed determined by two reactions affecting the scattering in opposite directions. (2) The first reaction is rapid, but the second may be slowed down by choosing appropriate assembly conditions. This allows the contributions to be analyzed separately. (3) Structurally the first phase of the undershoot may be interpreted in terms of partial ring breakdown, while the beginning of the rising phase corresponds to the association of oligomers. (4) The observed phases are closely reminiscent of the assembly induced by the slow T scan described previously (Bordas et al., 1983), in spite of the 60-fold difference in heating rate (2 deg/s and 2 deg/min, respectively). This suggests that similar structural transitions take place in the two conditions. (5) The effective temperature measured at the onset of assembly is variable (e.g., 26 °C in Figure 2c and 35 °C in Figure 2d), reflecting the lag due to prenucleation and nucleation events. By contrast, disassembly sets in rather reproducibly at a temperature just below 20 °C, indicating a major change in microtubule stability around this temperature [compare Johnson and Borisy (1979)].

Separation of Prenucleation and Nucleation Events. When surveying different assembly conditions, we found that the separation of prenucleation and nucleation events depended on the protein preparation but could be achieved rather reproducibly by lowering the ionic strength and pH. The experiments to be described now have been performed with the same protein preparation as in Figure 2 but were carried through another cycle in order to change buffer conditions. Figure 3a shows the time courses of the intensities at various scattering angles of a sample in 0.05 M PIPES buffer, pH 6.5. In these conditions, the undershoot reaches equilibrium before the onset of assembly. Setting the initial state equal to 1.0, the intensity drops to 0.81 during the undershoot, rises 1.4-fold during the final assembly, and drops to its initial value after one cycle (not shown). In the region of the ring scatter, the intensity drops continuously with clear separation of two phases, first to 0.82 and then to 0.31 of the initial level. The difference curve (Figure 3b, bottom) shows that the intensity decay is due to the disappearance of rings. Moreover, comparison with model curves based on oligomers (Figure 1) shows that the products of ring disassembly must be small, probably down to the size of dimers (this follows from the roughly proportional decay of the scattering trace up to about 0.08 nm^{-1}). The side maxima of the initial ring scattering occur at about 0.033 and 0.064 nm^{-1}, indicating a mean diameter of about 36 nm, i.e., similar to the sizes found in standard conditions.

Microtubule assembly starts at an apparent temperature of 26 °C, or 16 s after initiating the T jump. The longer delay compared with the previous experiment (Figure 2c) is one of the factors explaining the large undershoot. The second factor is the higher initial concentration of rings. This can be shown as follows. We scale the experiments of Figures 2 and 3 with respect to the total mass of assembled microtubules and then compare the initial cold states. The difference curve (Figure 3b, top) shows the pattern characteristic of rings, and the intensities indicate that there are about 50% more rings at the lower ionic strength and pH. This means that these conditions favor the formation of rings at low temperature but do not protect them against temperature-induced disassembly. The experiment also shows a correlation between higher (initial) stability of rings and a delay of nucleation, supporting the view that ring formation and microtubule formation represent antagonistic reactions.

The apparent half-time of ring breakdown is about 10 s. Close inspection of the intensity decay shows that it is nearly

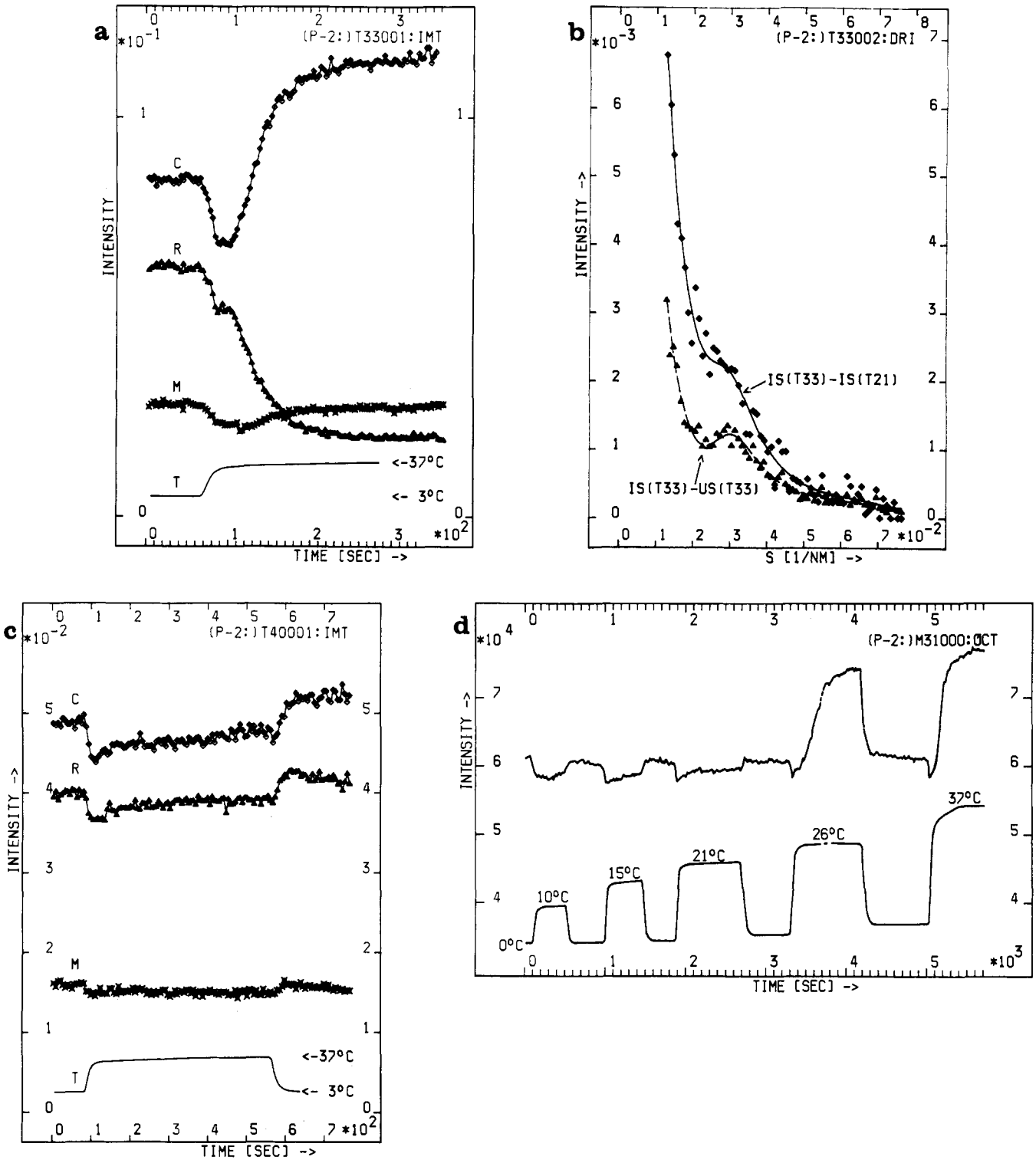

FIGURE 3: Assembly of microtubule protein C_4S-56 prepared from the protein used for Figure 2 by another cycle of assembly and resuspending the pellet in 0.05 M PIPES, pH 6.5, and the other factors as above. Protein concentration 22 mg/mL. (a) Experiment T33.830, time courses of central, ring, and microtubule scatter and temperature (same symbols as in Figure 2c). Note that the ratio of final to initial level is low, 1.4 compared to the usual ratio of about 2 (Figure 2c), indicating a higher initial degree of polymerization [mainly due to rings, see (b)]. By contrast, the intensity ratio of final level vs. undershoot is 1.4/0.8 = 1.75, close to the standard value. (b) Difference scattering curves. The bottom curve [IS(T33) – US(T33)] is the difference of the initial state of T33.830 and the bottom of the undershoot (Figure 3a), illustrating the breakdown of rings into small oligomers and dimers. The top curve [IS(T33) – IS(T21)] is the difference between the initial cold state of T33.830 and T21.829 (Figure 2c), scaled on the basis of their patterns after microtubule assembly (the pattern at 37 °C of T33.830 can be superimposed on that of T21.829 when a scale factor of 1.33 is applied to the latter). This shows that there are about 50% more rings at the lower ionic strength and pH. (c) Experiment T40.830, time courses of scattering as in (a). Microtubule protein C_4S-53 prepared as in (a) except that GTP was omitted. One observes the temperature-dependent partial ring breakdown and re-formation without interference from microtubule assembly. Every second data point is shown. (d) Experiments M31.OCT to M33.OCT, showing the time course of the central scatter during limited temperature jumps. Microtubule protein C_3S-14 in 0.1 M PIPES, pH 6.9, with 1 mM EGTA, GTP, and DTT, 26 mg/mL. The low temperature was kept at 0 °C, and the high temperature was set at 10, 15, 21, 26, and 37 °C during successive cycles. Every T jump induces the reversible disassembly of rings, but only the last two cycles cause microtubule assembly.

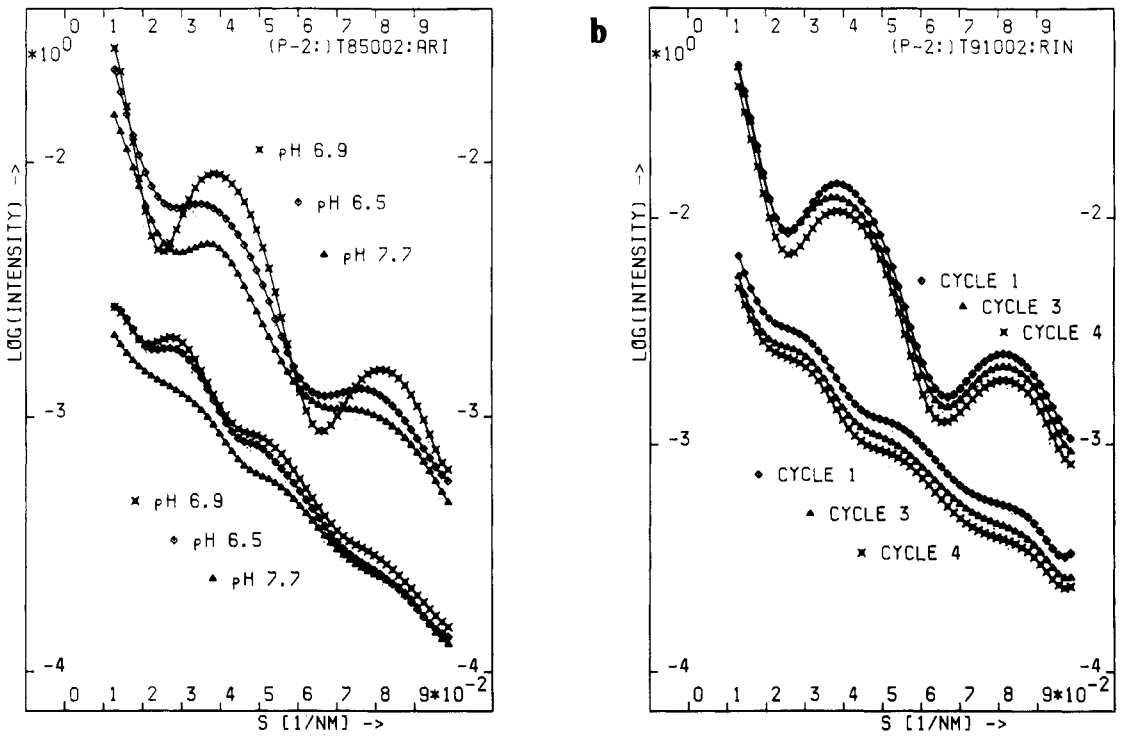

FIGURE 4: Comparison of the effects of pH and assembly cycles on the X-ray scattering. Every second data point is shown. (a) Effect of pH. (Bottom) The three curves show the scattering of solutions at 4 °C at pH 6.9, 6.5, and 7.7 (in descending order; experiments T85.705, T81.705, and T84.705, respectively, preparation C_4S-36, 19 mg/mL, all in 0.1 M PIPES buffer, including 1 mM EGTA, GTP, and DTT). The subsidiary maxima typical of rings of about 38-nm diameter are seen most clearly at pH 6.9 (the curves shown have been averaged over 50 s and smoothed by cubic splines). At pH 7.7, the ring scattering is greatly reduced, and the maxima are shifted to the right, corresponding to a mean diameter around 36 nm. (Top) Scattering of same three preparations after microtubule assembly, same descending order in the region of the subsidiary maximum typical of microtubules. Note that the maxima and the contrast between the minima are most clearly expressed at pH 6.9 and least clearly expressed at pH 7.7. In this preparation, the main peaks are around 0.04 nm^{-1}, corresponding to a mean diameter of 28 nm (probably due to a larger mean number of protofilaments and possibly to the influence of MAPs on the outer surface). The top curves have been shifted up by 0.75 log unit (factor 5.6) for better visibility. Despite the differences in structure, all three experiments show similar rates for the prenucleation and assembly phases (lag time 15–20 s, half-time of assembly 6–10 s, progress curves not shown). (b) Assembly cycles. This plot is similar to (a), the three bottom curves showing the scattering of the cold solution before the first, third, and fourth cycles (in descending order) and the three top curves being from microtubules assembled in these cycles (raised by 0.75 log unit and smoothed by spline functions). Experiments T88.705, T90.705, and T91.705, preparation C_3S-35, 0.1 M PIPES, pH 6.9, including 1 mM EGTA, $MgSO_4$, and DTT and 5 mM GTP, 23 mg/mL [the excess GTP serves to reduce the inhibitory effect of GDP generated during the repeated cycles; thus the lag and assembly times are similar as in (a)]. In contrast to (a), the curves are nearly parallel, indicating that the structures dominating the patterns (rings, bottom; microtubules, top) decrease by about 10% with each cycle but the distribution of scatterers and their structure are preserved (this holds as long as the GTP/GDP ratio remains high).

linearly related to the temperature, both in fast temperature jumps and slow temperature scans [this is best shown by correlation plots; see Bordas et al. (1983)]. Thus the apparent rate does not represent a reaction rate but rather a temperature-dependent equilibrium between rings, oligomers, and dimers whose interconversion is faster than the T jump employed here. This explains why the breakdown of rings produced by the temperature rise itself is only partial in the temperature range studied here.

This point is illustrated in Figure 3c where GTP was omitted from the buffer. One observes a temperature-induced drop in the intensities similar to that of the undershoot before. However, there is no subsequent assembly phase (apart from a small degree of unspecific aggregation), and the scattering returns close to the initial level when the temperature is dropped, with a rate that parallels the temperature change. Thus, it appears that complete dissolution of rings requires microtubule assembly.

Another way to separate prenucleation events from assembly is to apply limited temperature jumps, as illustrated in Figure 3d. In this experiment, the protein was cycled several times. The low temperature was kept at 0 °C, while the high temperature was initially set at 10 °C and increased in several steps during successive cycles (i.e., 10, 15, 21, 26, and 37 °C). In this example, the temperatures of the first three cycles are not sufficient to initiate assembly so that one observes only the prenucleation events. Microtubules are formed during the fourth and fifth cycles, preceded as before by the undershoot due to prenucleation breakdown of oligomers.

In summary, the experiments of Figure 3 illustrate that the different reactions of the protein following a temperature jump may be separated in several ways, whose common feature is to prevent or retard the onset of nucleation.

Effect of pH and Cycling on Oligomeric and Polymeric States. The distribution of oligomers of microtubule protein depends on solution conditions. Using analytical ultracentrifugation, Marcum and Borisy (1978) showed that low pH, low ionic strength, and high protein concentration favored a 30S species (rings), whereas higher pH (>7) and ionic strength caused its disintegration into 18S oligomers and 6S dimers. Since we were interested in the role of oligomers during assembly, we performed X-ray experiments in similar solution conditions. The protein was prepared by two cycles in standard conditions (0.1 M PIPES, pH 6.9) and adjusted to the desired pH during a third cycle.

Figure 4a (top) shows the scattering traces after assembly at pH 6.5, 6.9, and 7.7 in 0.1 M PIPES reassembly buffer. The clearest pattern (in terms of contrast between maxima and minima) is obtained at pH 6.9; it is dominated by the scattering of microtubules of 28-nm mean diameter. The other

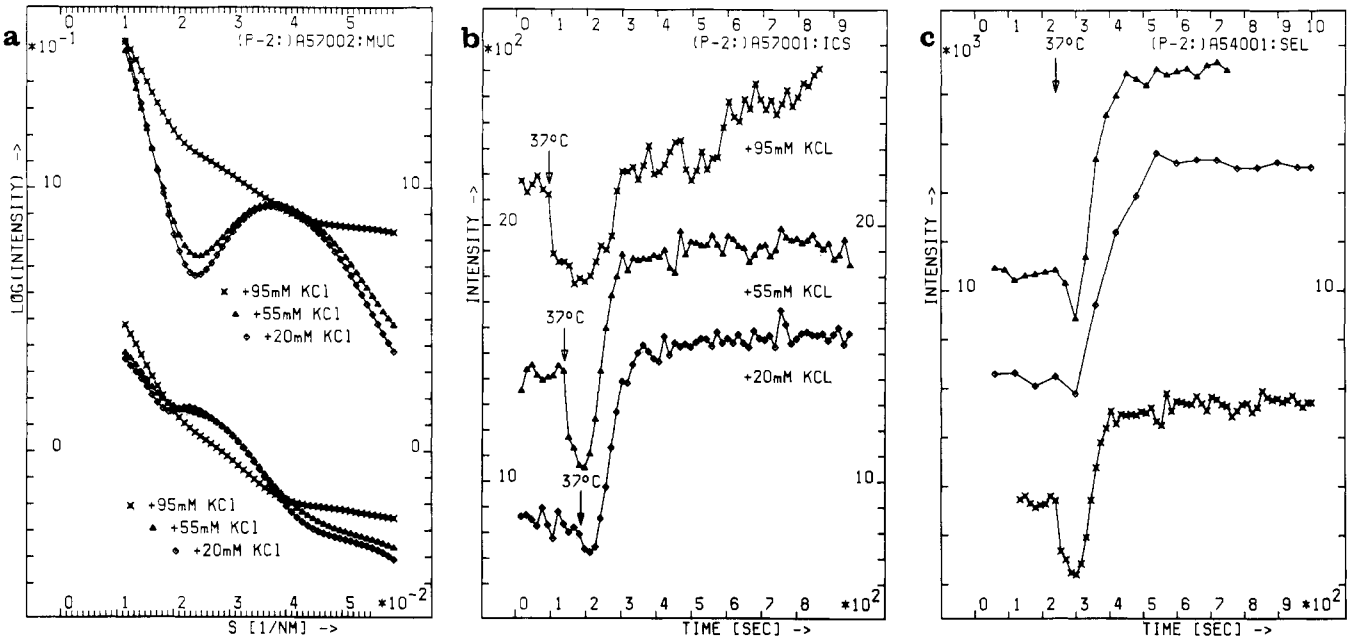

FIGURE 5: Dependence of scattering on increasing ionic strength at constant pH 6.6. Preparation C_3S-M, 20 mg/mL, 0.05 M PIPES, pH 6.6, adjusted with KOH with 1 mM GTP, DTT, EGTA, and $MgSO_4$ and various amounts of salt added. Experiments A50.AUG (+20 mM KCl), A54.AUG (+55 mM KCl), A57.AUG (+95 mM KCl). (a) Scattering traces at low and high temperature. (Top, 37 °C) The microtubule pattern is most clearly expressed in run A50.AUG (+20 mM KCl, diamonds); it becomes somewhat blurred at higher added salt concentrations (run A54.AUG, +55 mM KCl, triangles) but is completely extinguished at 95 mM KCl (run A57.AUG, crosses). (Bottom, 4 °C) The ring pattern is seen at the two lower salt concentrations (A50.AUG, diamonds; A54.AUG, triangles) with the steeper slope of A50.AUG indicating a higher fraction of double rings. At 95 mM added KCl, the ring pattern disappears and is replaced by a smoothly decaying curve typical of oligomers (A57.AUG, crosses). The curves at 37 °C are shifted up 1 log unit compared to the 4 °C curves. (b) Time courses of central scatter in the experiments shown in (a). With 20 and 55 mM KCl added, one observes normal microtubule assembly, but note the clearer appearance of the undershoot with 55 mM KCl. With 95 mM KCl added, there is an extended undershoot (indicating partial breakdown of oligomers), followed by a gradual aggregation that does not reach equilibrium during the experiment and does not result in microtubule assembly, as shown in (a). (c) Effect of different monovalent ions on time course of central scatter at pH 6.6. (Top) Experiment A33.AUG, preparation C_3S-M in 0.05 M PIPES, pH 6.6, adjusted with NaOH with 1 mM EGTA, DTT, GTP, and $MgSO_4$ and 40 mM NaCl added. (Center) Experiment A30.AUG, same preparation as (a), but buffer adjusted with KOH and 40 mM NaCl added. (Bottom) Experiment A54.AUG, same preparation as before, but buffer adjusted with KOH and 55 mM KCl added. Note the smaller undershoot in the presence of Na^+ (top and center curves).

patterns are less contrasty and indicate an increasing contribution from non-microtubular aggregates. This is particularly apparent at pH 7.7. Considering that the pH optimum of assembly is below 7, it is in fact remarkable that microtubules are formed at all; this is explained by the high protein concentration used here, which exceeds the critical concentration at high pH [around 2 mg/mL; see Regula et al. (1981)].

In the case of the cold solutions (Figure 4a, bottom), the curves at pH 6.9 and 6.5 show clear maxima arising from rings. The middle curve (pH 6.5) decays more rapidly, as expected from a larger fraction of double rings, compared to pH 6.9 (in agreement with electron microscopy, not shown; see Figure 1). Note that the single and double rings have similar mean diameters (about 38 nm). By contrast, the maxima at pH 7.7 are strongly reduced, indicating that rings break apart at higher pH values and give rise to other oligomeric structures, as seen from the slope of the traces (as before, the fact that some rings are observed is due to the high protein concentration).

In spite of the differences in assembly forms, the kinetics are similar at the three pH values studied; little undershoot is visible, and the half-time of assembly is about 15 s. In other words, the high pH at 0.1 M PIPES reduces the extent of microtubule assembly but not the rate of nucleation. This is in contrast to the effect of lowering the buffer strength to 0.05 M, which slows down nucleation but has a lesser effect on the extent of assembly (see Figure 3).

In order to highlight the difference in scattering induced by pH, we show the response of the same protein preparation to repeated cycles of assembly and disassembly (Figure 4b), using a higher concentration of GTP (5 mM) in order to suppress the inhibitory effect of rising GDP. This example shows almost no deterioration of the pattern at low and high temperature; i.e., the contrast between the minima and maxima and the positions of the peaks remains nearly unaltered. The main change is a gradual decrease of the polymerizable material that causes the curves to run nearly parallel in a logarithmic plot (apart from some aggregation contributing to the very low angle region). Likewise, the kinetics of assembly and disassembly show little change up to the fourth cycle.

Influence of Monovalent Cations. The separation of prenucleation and nucleation events illustrated in Figure 3a was achieved by lowering the ionic strength via the buffer, thereby retarding assembly. A similar effect can be produced by raising the ionic strength beyond the assembly optimum. Figure 5 (parts a and b) shows an example where different concentrations of KCl were added to a protein sample prepared in 0.05 M PIPES at pH 6.6. Up to about 70 mM added salt, there is little effect on the half-time of assembly, although the apparent undershoot becomes more pronounced. However, at 95 mM added salt, one observes a clear separation of the prenucleation events, followed by a slow and a biphasic assembly process (Figure 5b). The scattering curves (Figure 5a) show that the high salt concentration leads to a breakdown of rings into other oligomeric structures and a concomitant loss of microtubule assembly; i.e., the rise in the central scatter observed at 95 mM KCl following the temperature jump (Figure 5b, top) is due to nonspecific aggregation.

Figure 5c illustrates that these effects depend not only on

ionic strength but also on the nature of the cations. The clearest separation of the phases at intermediate concentrations of added salt is seen in the presence of K^+ (Figure 5c, bottom), whereas the presence of Na^+ appears to accelerate nucleation and thereby reduces the apparent undershoot (Figure 5c, center and top).

Other Factors Influencing the State of Oligomers. The figures shown thus far illustrate that the equilibrium between oligomeric states is affected by a variety of solvent conditions such as temperature, ionic strength, or pH, a complete map of which would result in a phase diagram analogous to that shown by Marcum and Borisy (1978) derived from analytical ultracentrifugation. It is clear that other factors may be equally important, as illustrated by the following two examples.

First, when microtubule protein is stored frozen in reassembly buffer lacking GTP, the concentration of rings after unfreezing is very low, even when GTP is added; instead, one observes a higher contribution from nonring oligomers. However, a cycle of assembly and disassembly restores the usual equilibrium between rings and oligomers (comparable to that shown in Figure 2b). Second, purified tubulin does not contain rings in the standard buffer, and only a few are formed when the cold protein is mixed with MAPs. However, the usual fraction of rings reappears after one cycle. These examples indicate that the history of the sample must be taken into account; the species generated by microtubule disassembly are not necessarily the same as those initiating assembly.

Discussion

Preassembly States of Tubulin. Despite much work on microtubule assembly in vitro, the nature of the entities that contribute to nucleation and elongation has remained rather elusive. Studies with brain microtubule protein showed that in conditions conducive to assembly one observes a variety of polymorphic forms (rings, sheets, helical ribbons, etc.). These led to models of nucleation based on the assumption that the polymorphic forms were precursors or intermediates [reviewed by Kirschner (1978)]. On the other hand, kinetic data supported models of elongation based on the endwise addition of subunits [e.g., Gaskin et al. (1974)]. Other workers investigated the assembly of purified tubulin and showed that it did not require the polymorphic intermediates. This pointed to the influence of MAPs, which not only stimulate assembly but also cause polymorphism, indicating that the relationship between the two effects may only be indirect. Finally, the demonstration that microtubule assembly was preceded by the disassembly of rings led to the view that oligomeric species smaller than rings contributed to nucleation and possibly to elongation (Engelborghs et al., 1977; Mandelkow et al., 1980; Weisenberg, 1980). Present discussions on microtubule assembly are largely centered on the mechanism of elongation or shortening, in particular the role of nucleotides and their possible implications in treadmilling (Margolis & Wilson, 1978) or dynamic instability (Mitchison & Kirschner, 1984). By contrast, the mechanism of nucleation and the events leading to it have received less attention, probably for want of a reliable assay. Small oligomeric structures can be observed by nondenaturing gel electrophoresis (Kravit et al., 1984), but the possible artifacts of this method leave the results ambiguous, as discussed by Lee et al. (1973) and Correia and Williams (1985). In this paper, we use the method of time-resolved X-ray scattering to study the fate of oligomers before and during assembly.

In earlier experiments employing a moderate temperature jump, we found that the assembly of microtubule protein was preceded by prenucleation events consisting largely of ring disassembly (Mandelkow et al., 1980). Near-equilibrium T-scan experiments showed that the subsequent nucleation could be described in terms of oligomer association (Bordas et al., 1983). It was not clear, however, what the relationship between the breakdown products of rings and the nucleating oligomers was. These experiments were performed in reassembly buffer with 0.1 M PIPES, pH 6.9, in which the prenucleation and nucleation events largely overlapped. We, therefore, attempted to find conditions where the two phases can be observed separately. This can be achieved in several ways, for example, by lowering the pH and the ionic strength, by reducing GTP, or by lowering the temperature jump. The main findings can be summarized as follows.

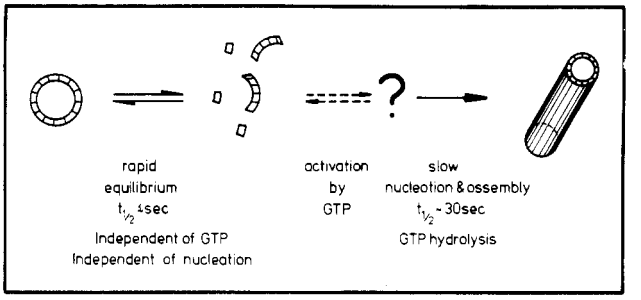

FIGURE 6: Diagram summarizing the differences between prenucleation and nucleation events. There is a rapid and reversible temperature-dependent equilibrium between rings, smaller oligomers, and dimers that is not directly related to microtubule assembly (left part of diagram). By contrast, microtubule nucleation and assembly are slow and take place above a threshold temperature (right part of diagram). Since the ring-forming and microtubule-forming modes of assembly draw on the same pool of building blocks (oligomers and dimers), one requires one or more intermediate steps during which the sunits are activated for assembly, e.g., by temperature and GTP. The structure(s) of the activated oligomers and dimers is (are) unknown but could correspond to straightened protofilament fragments, in contrast to the inactive coiled ones.

(*1*) *Temperature Dependence.* Under all conditions studied (including slow T scan and fast T jump), the prenucleation events were almost linearly correlated with temperature, i.e., the half-time of equilibration between rings and their disassembly products is in the range of seconds or less. In other words, the ring pattern can be (and was in fact) used as a thermometer to monitor the temperature of the solution. Thus, the formation of rings from their subunits is an exothermic process, in agreement with data derived from UV light scattering (Engelborghs et al., 1980).

(*2*) *Extent of Reaction.* Between 3 and 37 °C, the ring fraction decreases only by about 20%. Thus, the rings appear surprisingly stable, even at elevated temperature. Since the initial ring fraction is about 50–70% of the total protein in our concentration range, the enthalpy of ring formation from their subunits is on the order of a few kilocalories per mole. The complete disappearance of rings during microtubule assembly, therefore, requires processes other than temperature-induced ring breakdown. The simplest explanation would be the depletion of the subunit pool (small oligomers and dimers) by the nucleating species. This implies that there is an equilibrium of the form

$$\text{rings} \rightleftarrows (\text{oligomers} + \text{dimers}) \rightleftarrows \text{nuclei}$$

such that both rings and nuclei draw on the same pool (see Figure 6).

(*3*) *Reversibility.* Prior to assembly, the equilibrium between rings and their breakdown products appears to be reversible. By contrast, once nucleation sets in, the assembly cycle shows hysteresis [see Bordas et al. (1983)].

(*4*) *Nucleotides.* Their role and their dependence on Mg^{2+} will be described in more detail elsewhere, but we note some key features here. In the absence of GTP, one observes the reversible dissociation and association of rings (Figure 3c). In the presence of GTP, the same effect can be observed, provided that the temperature jumps remain below the point where nucleation sets in. This suggests that neither binding nor hydrolysis of GTP plays a role at the prenucleation stage.

(*5*) *Role of MAPs.* MAPs from mammalian brain support the formation of ring oligomers, but the efficiency is low unless the mixture of tubulin and MAPs is cycled. This indicates that MAPs bind to microtubules in a specific fashion such that subsequent disassembly generates preformed building blocks that then reassociate into rings [e.g., the coiled protofilament fragments observed by cryo electron microscopy; see Mandelkow and Mandelkow (1985)]. Although complete rings are not observed in cells, the tubulin–MAP building blocks may be functionally important, e.g., as storage and/or assembly units.

(*6*) *Relationship with Oligomers Observed by Analytical Ultracentrifugation.* It has been shown that low pH and low ionic strength favor the formation of rings (30 S and higher), while high pH and high ionic strength cause their breakdown into smaller units such as 18 S (Marcum & Borisy, 1978; Regula et al., 1981; Martin et al., 1982). This trend is confirmed by the X-ray data, although the disappearance of rings and microtubules at higher pH is less pronounced because of the high protein concentration used here.

(*7*) *Role of Microtubule Assembly Inhibitors.* There are a variety of conditions that prevent microtubule assembly without a major effect on ring stability. Two of these have already been mentioned, namely, low temperature and absence of GTP. Other examples are the presence of millimolar amounts of Ca^{2+} or GDP, which leave rings largely intact even at 37 °C (data not shown). It appears that conditions that are conducive to ring formation are detrimental for microtubule formation, and vice versa. This fact may be expressed more simply in structural terms: protofilament coiling (rings) is antagonistic to protofilament straightening (microtubules). One could turn the argument around by postulating that microtubule disassembly is caused by factors whose primary effect is to induce a coiled protofilament conformation, even when there is no ring-like closure of the protofilaments. Evidence in support of this comes from disassembly experiments with colchicine (Kirschner et al., 1974) or rapid freezing (Mandelkow & Mandelkow, 1985). Note that this interpretation rests on the view that tubulin oligomers consist of short protofilament fragments.

Oligomeric species other than rings are almost invariably observed by negative-stain electron microscopy of cold microtubule protein. Analytical ultracentrifugation tends to emphasize bimodal distributions between tubulin dimers (6 S) and rings (30 S and up), but intermediate species are observed as well. Some of these may be the result of isodesmic self-association [especially in the case of purified tubulin; see Frigon and Timasheff (1975)] while others appear to represent discrete assembly states that can be fixed and observed by electron microscopy [e.g., the 18S species of microtubule protein; Marcum and Borisy (1978)]. Small oligomers are particularly enriched during microtubule nucleation, as seen both by analytical ultracentrifugation (Weisenberg, 1974) and by electron microscopy (Bordas et al., 1983). As described here, nonring oligomers can also be enriched at the expense of rings by certain solution conditions such as high pH, high salt, or storage of the protein at low GTP or without MAPs. Oligomeric species of tubulin are seen on nondenaturing gels (Lee et al., 1973) and have been implicated in microtubule assembly (Kravit et al., 1984). Finally, the participation of tubulin–MAP oligomers in the nucleation of microtubule protein is suggested by the low apparent cooperativity (n = 2; Engelborghs et al., 1977), compared with that of purified tubulin (n = 12; Carlier & Pantaloni, 1978).

The sum of these observations is somewhat contradictory. On the one hand, nonring oligomers appear to play a role in microtubule nucleation; on the other hand, conditions that inhibit microtubule assembly favor the formation of nonring oligomers. This is best explained by assuming that there are different types of oligomers, active and inactive ones. Active oligomers would contribute to microtubule nucleation and possibly elongation. Inactive oligomers could consist of partially denatured protein, as suggested by Correia and Williams (1985). Alternatively, oligomers may be temporarily inactivated, e.g., by binding of assembly inhibitors such as GDP or Ca^{2+} or at low temperature, but may be reactivated by removing these ligands, replacing them by activators (e.g., GTP), or raising the temperature. Structurally, an inactive oligomer may be viewed as a coiled protofilament fragment that would be straightened as a result of activation.

The continuity between the prenucleation and nucleation events observed previously (Mandelkow et al., 1980) suggested that there was a direct conversion from ring breakdown products to microtubule nuclei. Since the two phases can be separated, it appears now that there must be additional intermediate steps, i.e., breakdown of rings into oligomers or dimers is not sufficient to cause microtubule assembly (and vice versa). This is best explained if we make the following assumptions: (1) The ring-forming and microtubule-forming modes of assembly are not directly linked to one another [this would be in analogy with the disk-forming and helix-forming modes of assembly of the well-known example of tobacco mosaic virus protein; see Lauffer (1975)]. (2) Both assembly forms draw on the same pool of intermediates, i.e., oligomers and dimers. (3) The intermediates can be activated or inactivated for the respective modes of assembly by binding of ligands (e.g., GDP, GTP, etc.). Thus, a minimal reaction scheme would be

$$\text{rings} \rightleftarrows (\text{oligomers} + \text{dimers})_C \rightleftarrows (\text{oligomers} + \text{dimers})_S \rightleftarrows \text{nuclei}$$

in which subscript C ("coiled") refers to the oligomeric state that is active for ring formation but inactive for microtubule assembly and subscript S ("straight") refers to the state that is active for microtubule assembly (Figure 6).

Acknowledgments

We gratefully acknowledge the important contributions of our colleagues to the project: P. Maier (MPI) for building the T-jump cell, E. Dorrington (EMBL) for the electronic control modules, J. Hendricks (EMBL) for providing the position-sensitive detector, U. Rühl (MPI) for protein preparations, and M. Koch (EMBL) for discussions and computer programs for data processing.

References

Bordas, J., Koch, M. H. J., Clout, P. N., Dorrington, E., Boulin, C., & Gabriel, A. (1980) *J. Phys. E 13*, 938–944.

Bordas, J., Mandelkow, E.-M., & Mandelkow, E. (1983) *J. Mol. Biol. 164*, 89–135.

Borisy, G. G., Marcum, J. M., Olmsted, J. B., Murphy, D. B., & Johnson, K. H. (1975) *Ann. N.Y. Acad. Sci. 253*, 107–132.

Carlier, M. F., & Pantaloni, D. (1978) *Biochemistry 17*, 1908-1915.
Correia, J. J., & Williams, R. C. (1985) *Arch. Biochem. Biophys. 239*, 120-129.
Engelborghs, Y., De Maeyer, L. C. M., & Overbergh, N. (1977) *FEBS Lett. 80*, 81-85.
Engelborghs, Y., Robinson, J., & Ide, G. (1980) *Biophys. J. 32*, 440-443.
Frigon, R. P., & Timasheff, S. N. (1975) *Biochemistry 14*, 4559-4566.
Gabriel, A. (1977) *Rev. Sci. Instrum. 48*, 1303-1305.
Gaskin, F., Cantor, C. R., & Shelanski, M. L. (1974) *J. Mol. Biol. 89*, 737-758.
Guinier, A., & Fournet, G. (1955) *Small-Angle Scattering of X-rays*, Wiley, New York.
Hendrix, J., Koch, M. H., & Bordas, J. (1979) *J. Appl. Crystallogr. 12*, 467-472.
Johnson, K. A., & Borisy, G. G. (1979) *J. Mol. Biol. 133*, 199-216.
Kirschner, M. W. (1978) *Int. Rev. Cytol. 54*, 1-71.
Kirschner, M. W., Williams, R. C., Weingarten, M., & Gerhart, J. (1974) *Proc. Natl. Acad. Sci. U.S.A. 71*, 1159-1163.
Koch, M. H. J., & Bendall, P. (1981) *Proceedings of the Digital Equipment Computer User Society*, pp 13-16, Digital Equipment Corp., Warwick, U.K.
Koch, M. H. J., & Bordas, J. (1983) *Nucl. Instrum. Methods Phys. Res. 208*, 461-469.
Kravit, N. G., Regula, C. S., & Berlin, R. D. (1984) *J. Cell Biol. 99*, 188-198.
Lauffer, M. A. (1975) *Entropy-Driven Processes in Biology*, Springer-Verlag, Berlin.
Lee, J. C., Frigon, R. P., & Timasheff, S. N. (1973) *J. Biol. Chem. 248*, 7253-7262.
Mandelkow, E., Mandelkow, E.-M., & Bordas, J. (1983) *J. Mol. Biol. 167*, 179-196.
Mandelkow, E.-M., & Mandelkow, E. (1985) *J. Mol. Biol. 181*, 123-135.
Mandelkow, E.-M., Harmsen, A., Mandelkow, E., & Bordas, J. (1980) *Nature (London) 287*, 595-599.
Marcum, J. M., & Borisy, G. G. (1978) *J. Biol. Chem. 253*, 2825-2833.
Margolis, R. L., & Wilson, L. (1978) *Cell (Cambridge, Mass.) 13*, 1-8.
Martin, S. R., Clark, D. C., & Bayley, P. M. (1982) *Biochem. J. 203*, 643-652.
Mitchison, T., & Kirschner, M. (1984) *Nature (London) 312*, 237-242.
Regula, C. S., Pfeiffer, J. R., & Berlin, R. D. (1981) *J. Cell Biol. 89*, 45-53.
Renner, W., Mandelkow, E.-M., Mandelkow, E., & Bordas, J. (1983) *Nucl. Instr. Methods Phys. Res. 208*, 535-540.
Schachterle, G. R., & Pollack, R. L. (1973) *Anal. Biochem. 51*, 654-655.
Weisenberg, R. C. (1974) *J. Supramol. Struct. 2*, 451-465.
Weisenberg, R. C. (1980) *J. Mol. Biol. 139*, 660-677.

Role of Cysteine Residues in the *Lac* Permease of *Escherichia coli*

Donald R. Menick,[‡] Jonathan A. Lee,[‡] Robert J. Brooker,[§] T. Hastings Wilson,[§] and H. Ronald Kaback*[,‡]

Roche Institute of Molecular Biology, Roche Research Center, Nutley, New Jersey 07110, and Department of Physiology and Biophysics, Harvard Medical School, Boston, Massachusetts 02115

Received September 24, 1986

ABSTRACT: Oligonucleotide-directed, site-specific mutagenesis has been utilized to replace cysteine residues 117, 333, or 353 and 355 with serine in the *lac* permease of *Escherichia coli*. Replacement of Cys-117 or Cys-333 has no significant effect on permease activity, while permease with serine residues in place of Cys-353 and Cys-355 has about 50% of wild-type permease activity. The results provide a clear demonstration that cysteine residues at positions 117, 333, 353, and 355 are not obligatory for lactose/H^+ symport. When considered in conjunction with previous findings, the results indicate that, of the eight cysteine residues in the *lac* permease, only Cys-154 is important for lactose transport. As discussed, the conclusion has important implications for the hypothesis that sulfhydryl–disulfide interconversion plays an important role in the symport mechanism.

The *lac* permease of *Escherichia coli* is an integral membrane protein encoded by the *lac Y* gene that catalyzes symport (i.e., cotransport) of β-galactosides with H^+ [cf. Kaback (1986) and Wright et al. (1986) for recent reviews]. The *lac Y* gene has been cloned and sequenced, and the permease has been purified to a single polypeptide species in a completely functional state, thereby demonstrating that the *lac Y* gene product is solely responsible for β-galactoside transport. Secondary structure models for the permease based on circular dichroic and laser Raman spectroscopy and on analyses of sequential hydropathic character suggest that the polypeptide is organized into 12–14 hydrophobic α-helical segments that traverse the membrane in a zig-zag manner, connected by more hydrophilic, charged segments. Preliminary evidence supporting certain general aspects of these models has been obtained from limited proteolysis studies and from binding studies with monoclonal and site-directed polyclonal antibodies.

During the past few years, oligonucleotide-directed, site-specific mutagenesis has been utilized to modify the structure and function of the *lac* permease (Sarkar et al., 1986a), and recent studies suggest that the technique has the potential to yield unique mechanistic information. Thus, a series of experiments utilizing site-directed mutagenesis (Padan et al., 1985; Püttner et al., 1986; Carrasco et al., 1986) has provided

* Correspondence should be addressed to this author.
‡ Roche Research Center.
§ Harvard Medical School.

0006-2960/87/0426-1132$01.50/0